JOURNAL OF GEOPHYSICAL RESEARCH, VOL. 90, NO. B9, PAGES 7837–7847, AUGUST 10, 1985

Complex Resistivity Measurements of Confined Rock

DAVID A. LOCKNER AND JAMES D. BYERLEE

U.S. Geological Survey, Menlo Park, California

Complex resistivity was measured for samples of Westerly granite and Berea sandstone saturated with 0.01 M KCl_{aq}. A four-electrode technique was employed to make measurements over a frequency range of 10^{-3} to 10^{6} Hz and a confining pressure range of 0.2 to 200 MPa. When the electrical response was analyzed in terms of equivalent conductivity σ' and relative permittivity K', both of these quantities varied more with confining pressure for the granite samples than they did for the sandstone. In addition, both rock types exhibited large low-frequency dispersion of permittivity. While previous studies have measured the response of near-dc conductivity to changes in pressure, measurements of pressure dependence of the full complex resistivity $\rho^*(\omega)$ provide greater insight into earthquake-related phenomena as well as induced polarization measurements and other remote sensing techniques.

INTRODUCTION

Induced polarization (IP) has been widely used in prospecting for disseminated sulfides as well as other ore bodies [*Sumi*, 1961; *Keller and Frischknecht*, 1966; *Madden and Cantwell*, 1967; *Wong*, 1979; *Nelson and Van Voorhis*, 1983]. Deeper crustal sounding techniques have also been used to study large geothermal systems as well as the roots of volcanoes or earthquake zones [*Stanley et al.*, 1977; *Hermance and Pedersen*, 1980]. In the field of earthquake prediction, resistivity studies have been used to search for stress changes and strain related to earthquakes [*Morrison*, 1978; *Rikitake and Yamazaki*, 1979; *Madden*, 1983]. Numerous laboratory studies have been conducted to make precise measurements of electrical properties of rock samples to understand the mechanisms that control the electrical response of rocks as well as to aid in the interpretation of field data. These studies are reviewed in the work of *Olhoeft* [1980] and *Parkhomenko* [1982]. *Brace and Orange* [1968] and *Brace* [1971] have studied the effect of confining pressure on the resistivity of rock at 10 Hz as well as the effects of stress [*Brace and Orange*, 1966] and implications for coseismic changes [*Brace*, 1975]. Other investigators have measured the frequency dependent complex resistivity ρ^* of rock and other geological materials [*Olhoeft*, 1980; *Arulanandan and Mitchell*, 1968; *Saint-Amant and Strangway*, 1970; *Shahidi et al.*, 1975] including studies of materials with varying degrees of saturation and at elevated temperatures [*Frisillo et al.*, 1975; *Ucok*, 1979; *Olhoeft*, 1979*a*, 1981; *Parkhomenko*, 1982].

In an attempt to develop a reliable tool for predicting earthquakes, many phenomena have been studied, including seismicity, well level changes, tilt, local magnetic fields, radon, ground potential, and animal behavior. The rationale for expecting measurable changes in these varied parameters is that they are all either directly or indirectly linked to regional changes in stress or strain which in turn are related to an impending earthquake. It has long been known that the electrical response of materials varies over an extremely broad range. For example, under various geological conditions, the resistivity of granite can vary by over 12 orders of magnitude [*Olhoeft*, 1981]. Because the electrical response of saturated and partially saturated rock is intimately related to its pore structure, changes in stress or strain that affect that structure can be expected to have measurable effects on electrical properties.

The work presented here is the first in a series of studies aimed at furthering our understanding of the effects of confining pressure and stress on the electrical response of partially and fully saturated rock. Because of the complex behavior of clays and other fault gouge materials, much work is needed in this area. As a first step, the present study is restricted to investigation of the pressure response of two less complex systems, namely, wet granite and sandstone.

NOMENCLATURE

The quantities used in this paper are essentially those discussed by *Von Hippel* [1954]. If a sample is subjected to a sinusoidally varying electric field **E**, a current of density **J** will, in general, flow in the sample. The field and current density can be related for a linear isotropic material through a complex conductivity

$$\sigma^* = \sigma' + i\sigma'' \tag{1}$$

where $i = (-1)^{1/2}$. We will use the convention that quantities with an asterisk are complex, consisting of real (prime) and imaginary (double prime) parts. Then

$$\mathbf{J} = \sigma^*\mathbf{E} \tag{2}$$

At this point, no distinction is made as to the mode of current flow, i.e., polarizing currents or conduction through free charge carriers. By defining complex permittivity

$$\varepsilon^* = \varepsilon' - i\varepsilon'' = \sigma^*/i\omega \tag{3}$$

where $\omega = 2\pi f$ is angular frequency, (2) can be rewritten as

$$\mathbf{J} = (i\omega\varepsilon' + \omega\varepsilon'')\mathbf{E} \tag{4}$$

Complex relative permittivity is defined as

$$K^* = K' - iK'' = \varepsilon^*/\varepsilon_0 \tag{5}$$

where ε_0 is permittivity of free space, and complex resistivity is

$$\rho^* = \rho' - i\rho'' = (\sigma^*)^{-1} \tag{6}$$

Then dissipation factor D or loss tangent $\tan\delta$ can be expressed as

$$D = \tan\delta = \frac{\sigma'}{\sigma''} = \frac{\rho'}{\rho''} = \frac{K''}{K'} \tag{7}$$

Finally, the phase angle $-\phi$ by which the total current den-

Paper number 4B5257.

sity leads the electric field is given by

$$-\phi = \pi/2 - \delta \tag{8}$$

A mathematically equivalent naming convention is often used [*Olhoeft*, 1980] in which conduction current $\sigma_c^*\mathbf{E}$ and displacement current $\varepsilon_d^*(\partial\mathbf{E}/\partial t)$ are treated as physically distinct quantities. In this case, σ^* would be called total electrical conductivity, and we have

$$\sigma^* = (\sigma_c' + \omega\varepsilon_d'') + i(\sigma_c'' + \omega e_d') \tag{9}$$

In reality, the physically measurable quantities are σ' and σ''. In addition, we will show that the separation of the total current into complex conduction and complex displacement currents in (9) is inappropriate in development of the model that best fits our data. Consequently, we will use (1) for the remainder of this paper.

Experimental Method

The sample assembly employed in these experiments is shown in Figure 1. All samples are 25.4-mm-diameter cylinders with nominal lengths of 25.4 mm, although some experiments were performed on samples with lengths varying from 12.7 to 63.5 mm. The sample column consists of the sample sandwiched between 0.51-mm-long porous ceramic spacers, between platinum screen electrodes, then 6.4-mm-long porous ceramic spacers, Pt electrodes, and finally nonconducting dense ceramic end pieces. The top end piece contains a hole for passage of pore fluid. A Teflon tube is bonded to the top of the hole and passes out of the end plug to a pore fluid reservoir at atmospheric pressure. In this way, the entire sample assembly is electrically isolated from the pressure vessel and electrical ground. The porous ceramic spacers are made from Coors AHP99. They are 99% Al_2O_3 bonded with a borosilicate glass containing no Mg or Ca. They have 42% porosity and, when they are wet, can support confining pressure in excess of 200 MPa. The 0.51-mm ceramic spacers are used to prevent the electrodes from contacting the sample directly, thus avoiding the possibility of unwanted contact potentials developed between the electrodes and metal-bearing grains. Electrodes are Pt wire screen coated with Pt black to reduce electrode polarization. Because the Pt black is a delicate coating, the screens are rubbed between flat surfaces to remove the Pt black from the surfaces that contact the ceramic spacers, leaving Pt black only on the protected surfaces of the screens. Pt leads are brought out through the vinyl jacketing material, sealed with vinyl cement, and crimp connected to Cu leads before being brought out of the pressure vessel. The confining fluid used is 5-cSt viscosity silicone oil.

Most of the early measurements of resistivity of saturated rocks were carried out with two-electrode measuring systems. It is now recognized that below about 1kHz, and in some cases at much higher frequencies, the electrodes become polarized to such an extent that they contribute significant errors to the measurements. One strategy for reducing these errors has been to vary the sample length, thereby dividing the measured impedance into two parts, one that is constant and due to electrode effects and another that is proportional to the sample length and reflects the true impedance of the sample [*Schwan et al.*, 1962; *Scott et al.*, 1967]. Although this procedure can reduce the measurement errors, for frequencies below about 1 Hz, electrode impedance will commonly become so large that accurate determination of the sample impedance becomes impossible. The limitations of this and other techniques are discussed by *Schwan* [1963]. The solution

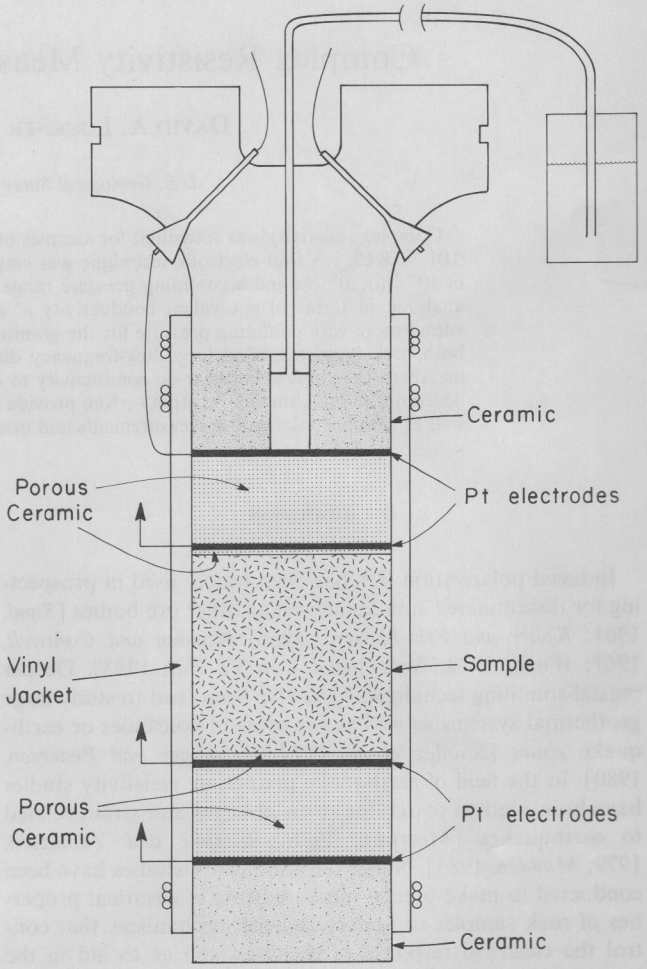

Fig. 1. Sample assembly for confined experiments. Sample is separated from Pt screen electrodes and nonconducting Al_2O_3 end caps by porous Al_2O_3 spacers.

that has generally been adopted to solve this problem is to use a four-electrode technique. Here the electrodes supplying current to the sample are physically separated from the electrodes used to measure the potential across the sample. By measuring the potential with a high input impedance, low noise current device, very little current is drawn through the potential electrodes, thereby minimizing the electrode polarization effects.

The measurement system we have employed in our experiments is essentially a duplicate of the four-electrode system described by *Olhoeft* [1979*a*]. Measurements were made in two modes. For high-frequency measurements, resistivity was measured with a two-electrode configuration (Figure 2*a*) using sequentially a Hewlett Packard 4275A (10 kHz to 1 MHz) and a 4274A (100 Hz to 100 kHz) LCR meter. As is shown in Figure 2*a*, the LCR meters require four input leads. However, they do not operate as a true four-lead system in the sense discussed above. Rather, they are designed so that when pairs of leads are connected at the sample, and the cable shields are connected appropriately, two advantages are gained. First, inductive noise that would otherwise be picked up by the leads is greatly reduced, and second, inductive and capacitive coupling of the leads can be measured and corrected for. The four-lead inputs to the 4274A and 4275A were joined at the end plug feed-throughs leading into the pressure vessel. In this way, cable effects up to this point were measured before each experiment and were automatically corrected for.

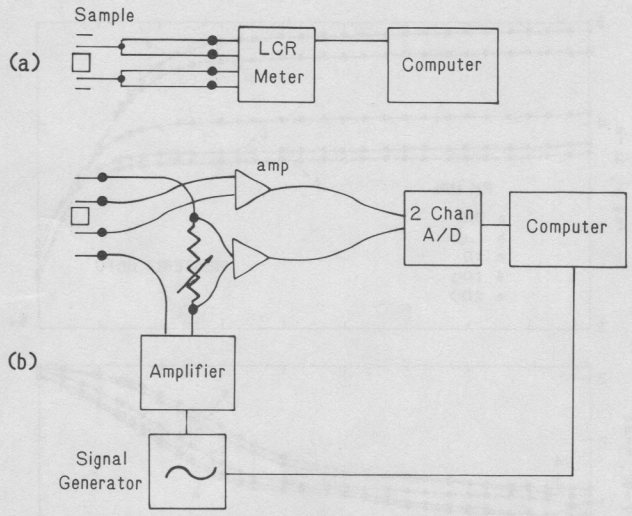

Fig. 2. Schematic diagram of measurement system. Upper diagram is for high-frequency measurements (10^2–10^6 Hz) using two-electrode technique; lower diagram is for low-frequency measurements (10^{-3}–10^2 Hz) using four-electrode technique.

For low-frequency measurements (10^{-3} to 10^2 Hz), a four-electrode system was employed as shown in Figure 2*b*. A Hewlett Packard 3325A signal generator was used to provide a 1-V peak-to-peak sine wave (LCR meters were also set to this voltage). This was buffered through a Crown DC-300A amplifier using unity gain and providing a bipolar output. The amplifier output was connected to the outer sample electrodes in series with a precision decade resistor. Because the decade resistor is preset to match the sample resistance, the voltage drop across the sample in all experiments is normally 0.5 V peak-to-peak. The voltage drop across the sample and the resistor were then amplified with Intronics IA294 high input impedance (3×10^8 ohms) isolation amplifiers, having low noise current, and active driven shields. The signals were sampled 128 times/cycle and analyzed in a Hewlett Packard 9845 computer for amplitude and phase relations as well as harmonic distortion. As we have already discussed, the high-frequency two-lead LCR measurements are susceptible to electrode polarization errors. Because these errors become progressively worse at lower frequencies, we always compared the LCR measurements in the 100- to 500-Hz range with independent measurements from the low-frequency four-electrode system. In this way, we are confident that the two-electrode measurements are being taken above the frequency range where significant polarization errors occur.

When the electrical properties of a system are analyzed according to a relation of the form given in (2), relating an input **E** to a response **J** through a transfer function σ^*, two general categories of response (linear and nonlinear) are observed. Two properties of a linear system are (1) the transfer function is independent of the amplitude of the input to the system, and (2) the output contains no new harmonic content. The usefulness of the distinction of linear and nonlinear systems can be seen in the nonlinear response of many clays which contains a wealth of information as to composition and particle size. For a more complete discussion of linearity in the electrical response of rocks, see *Olhoeft* [1979*b*]. In the current study, however, we are interested in the response of a low clay content sandstone and a granite. In this case, the root-mean-square difference between the harmonics in input and output waveforms is the total harmonic distortion (THD) and is a measure of the nonlinearity of the system.

Samples of Westerly granite and Berea sandstone were tested. All samples were presaturated with 0.01 *M* KCl_{aq} (7.1 ohm m) using deionized distilled water. This choice of electrolyte was in part arbitrary. The salt concentration was chosen to provide a resistivity within the general range of what might be encountered in groundwater. A single salt was chosen to give some control of chemical reactions that might occur in the samples, although NaCl could just as easily be used. Future studies will, in fact, include measurements of the effects of different electrolytes.

To saturate the samples, they were first evacuated and then pressurized in a beaker of the salt solution at 0.7-MPa pressure. The greatest care was taken with the granite samples which were evacuated for 5 days and pressurized for over 4 days. To study the effect of crack distribution on resistivity, one sample of Westerly granite, GR12, was altered in the following manner. The sample, with initial permeability $\eta = 100$ nanodarcies, was jacketed and placed under 80.0-MPa confining pressure and 78.0-MPa pore pressure. An additional axial load of 147 MPa was applied for approximately 1 hour and removed, after which permeability was found to have increased to 2000 nanodarcies. Pore pressure and confining pressure were then removed simultaneously so that the effective pressure never exceeded 2 MPa. A 25.4-mm sample of porous ceramic was also measured to test the system and to provide data necessary to correct for the thin 0.51-mm ceramic shims between the potential electrodes and the sample.

Measurement errors vary from experiment to experiment, depending upon the specific resistance and capacitance of the sample as well as the measuring instrument being used. Typical errors, computed from the manufacturer's specifications for the LCR meters and assuming 0.025% sampling error for the low-frequency measurements (12-bit A/D resolution) are as follows: errors in ρ' for granite samples typically vary with resistance and frequency and range from ± 0.3 to $\pm 3.0\%$ (>100 Hz) and ± 0.03 to $\pm 0.05\%$ (<100 Hz). For the sandstone, relative errors in ρ' similarly vary from ± 0.1 to $\pm 0.2\%$ (>100 Hz) and from ± 0.02 to $\pm 0.04\%$ (<100 Hz). Errors in measuring phase angle ϕ range, for granite, from ± 1.0 to ± 18.0 mrad (>100 Hz) and from ± 0.3 to ± 1.0 mrad (<100 Hz). For sandstone, errors in ϕ are ± 1.0 mrad (>100 Hz) and range from ± 0.3 to ± 1.0 rmad (<100 Hz).

Results

A typical run for the porous ceramic sample is shown in Figure 3. In this case, ρ' and $-\phi$ are plotted as a function of log frequency. The porous ceramic was selected because it is electrically neutral over the frequency range studied. This is confirmed by the fact that $\rho' = 31.0 \pm 0.05$ ohm m, independent of frequency. The phase angle diminishes from -68 mrad at 10^6 Hz to less than -1 mrad at 10^4 Hz, indicating a relative permittivity of $K' = 39 \pm 1$. A simple mixing law [*Olhoeft*, 1980],

$$K' = K_b^{(1-v)} \cdot K_w^{v} \tag{10}$$

where K_b is the high-frequency permittivity of the matrix material alone ($K_b = 12.6$ for corundum), K_w is the permittivity of the electrolyte (80), and v is porosity (0.42), predicts $K' = 27$. The discrepancy between predicted and measured values may be due to an additional contribution to the permittivity from interfacial polarization effects. This phenomenon will be discussed later. The total harmonic distortion, computed from the waveforms recorded by the low-frequency

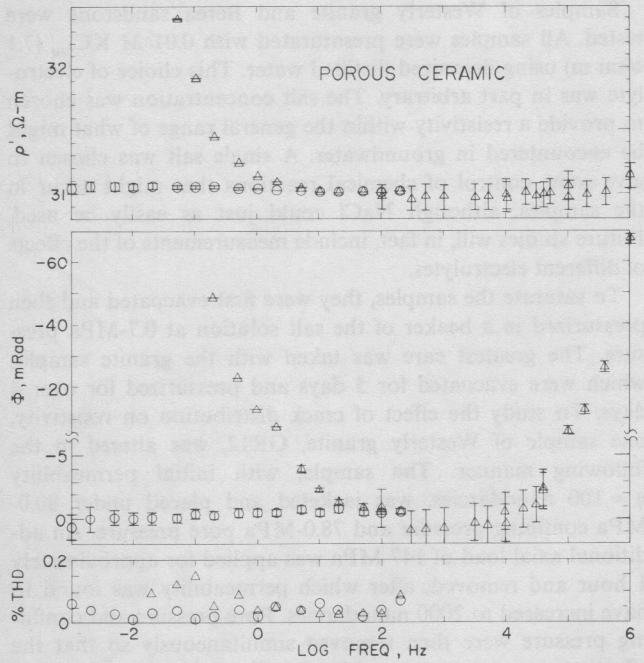

Fig. 3. Plot of ρ' and $-\phi$ versus log f for inert porous Al_2O_3 sample. Circles represent four-electrode measurements and triangles represent two-electrode measurements. Divergence of two- and four-electrode values below 10 Hz represents region where electrode polarization dominates two-electrode data. Parameter ρ' is independent of frequency over the entire range, while ϕ is measurably different from 0 only at high frequencies where dielectric behavior of the ceramic-electrolyte system becomes important. Total harmonic distortion (THD) is small, indicating linear response of sample.

system, were consistently below 0.05%. This further indicates that the brine-filled porous ceramic behaves as a linear system. In fact, THD for all samples was typically between 0.02 and 0.1%. When the ceramic sample was measured after 1 hour at 200 MPa, ρ' increased by 10%. Upon unloading, only 1.5% was recoverable, indicating a small but permanent collapse of the pore structure. A second series of measurements was conducted for the ceramic sample under identical conditions but using a two-electrode instead of a four-electrode low-frequency system. These results, also plotted in Figure 3, were used to test the effects of electrode polarization. The phase measurements of the two- and four-electrode systems begin to deviate below 50 Hz, while ρ' begins to differ below 5 Hz. This demonstrates the lower-frequency limit to which our two-electrode setup can be used even with the nonpolarizing Pt black electrodes.

Figures 4–6 plot ρ' and log $(-\phi)$ versus frequency for selected pressures in two granite and one sandstone experiments. The first granite sample (Figure 4) exhibited the greatest increase in both ρ' and $-\phi$ with increased confining pressure. This indicates a significant closing down of the interconnected pore space that provides a conductive path for the current flow. Data for the enhanced permeability granite sample, GR12, are shown in Figure 5. By comparison with Figure 4, we see that this sample behaved very much like the unaltered sample, GR10, and that the changes in crack geometry which were reflected in the increased permeability, had only a secondary effect on resistivity. These differences will be discussed in more detail later. The sandstone sample, BER10 (Figure 6), displayed a much smaller increase in ρ' and $-\phi$ with confining pressure than did the granite samples. We attribute this behavior to the fact that the sandstone matrix consists of

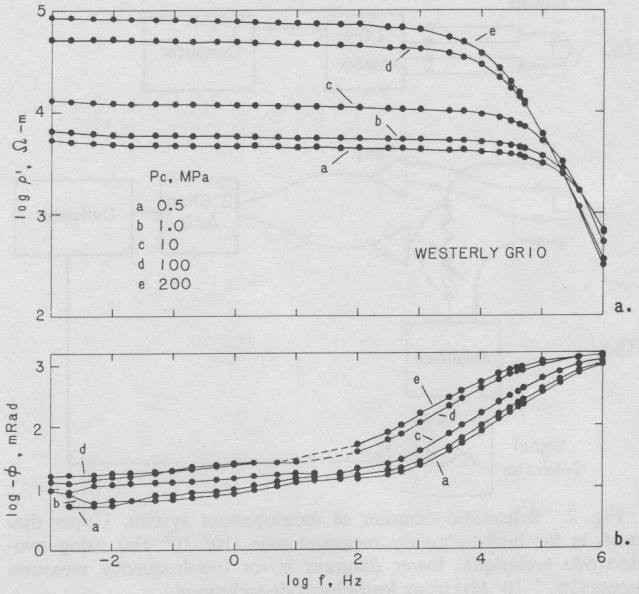

Fig. 4. Plot of log ρ' and log $-\phi$ versus log f for Westerly granite at selected confining pressures.

relatively well rounded grains which results in an open but strong structure. Consequently, there is only a small change in pore volume and surface area between 0.5- and 200-MPa confining pressure. Unlike the granite samples, the sandstone shows no detectable change in phase angle with confining pressure between 10^{-2} and 10^4 Hz. The increased scatter in phase angle below 10^{-2} Hz can be attributed to an increased noise level in the measuring system in this frequency range. This is evidenced by the fact that THD typically increases in this region. The small increase in phase angle at 0.1 Hz is in the range reported for some clay peaks [*Arulanandan and Mitchell*, 1968] and may be caused by the small percentage of clay found in this rock type. It is interesting to note that in the frequency range 0.1 to 100 Hz (the range over which IP measurements are generally made), approximately 1% of the

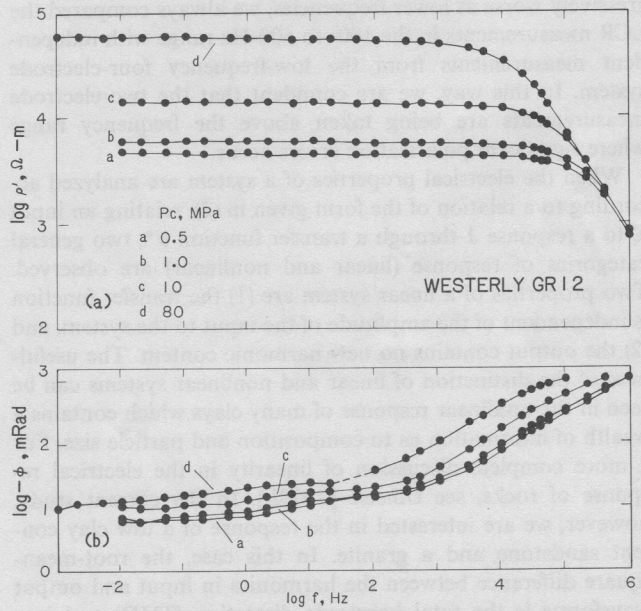

Fig. 5. Plot of log ρ' and log $-\phi$ versus log f for enhanced permeability Westerly granite sample.

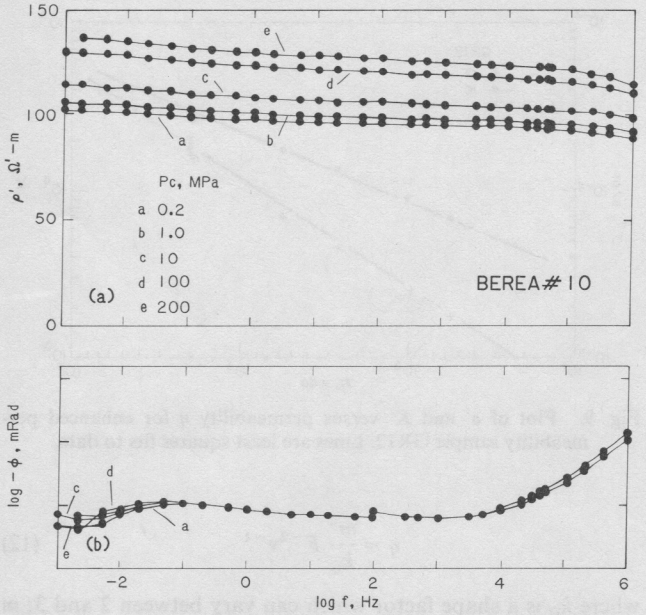

Fig. 6. Plot of ρ' and log $-\phi$ versus log f for Berea sandstone at selected confining pressures. Pressure effects are much smaller for sandstone than for granite samples.

total current is out of phase with the voltage (tan $\delta = 100$). This current, although small, can explain the background "noise" observed in IP measurements.

Using these same data, real conductivity σ' and real relative permittivity K' are plotted in Figures 7*a* and 7*b*. For sample GR10, low-frequency σ' drops off by 94% at 200 MPa, whereas the sandstone only decreases by 24%. The decrease in conductivity for the sandstone was fully recoverable upon unloading, whereas only 36% was recoverable for GR10. However, GR10 had not been allowed to equilibrate fully before the final measurements were made. This is evidenced by the fact that when unloaded to 10 MPa, σ' was still increasing during the final (10^{-2} to 10^{-3} Hz) measurements spanning about 30-min time. Nearly all measurements were taken after an equilibration time of 0.5 to 2 hours, although the decreasing pressure measurements for GR10 were taken after 15 min. The granite samples, when measured after a decrease in pressure, probably required days to equilibrate, since the external pore pressure was atmospheric pressure. A long recovery time for permeability of Westerly granite has been observed by C. A. Morrow et al. (private communication, 1985) and may reflect a time dependent process that would also contribute to recovery time of ρ'. Figures 7*a* and 7*b* show that at low frequencies the relative changes in σ' and K' with frequency for each sample have little pressure dependence. Consequently, in Figures 8*a* and 8*b*, σ' and K' are plotted as a function of confining pressure, using all data sets, at a representative frequency of 1 Hz.

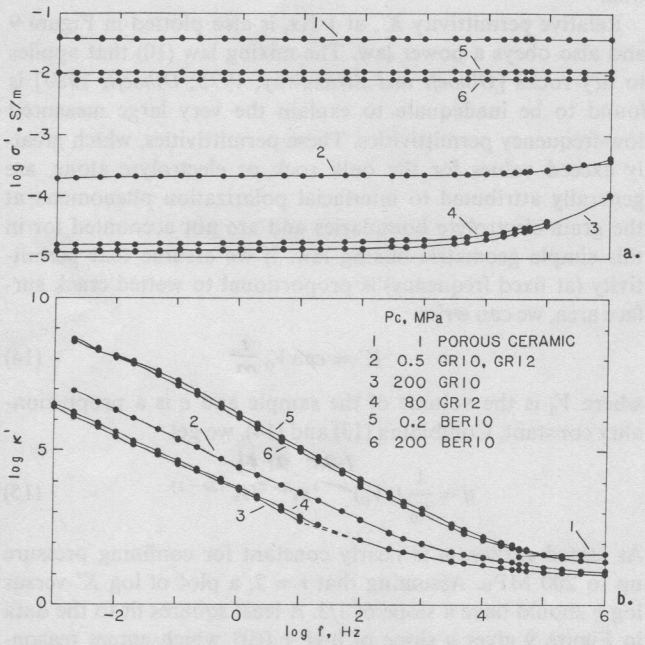

Fig. 7. Plot of (*a*) log σ' and (*b*) log K' versus log f for all samples at selected pressures. Conductivity has little frequency dependence below 10^4 Hz. Granite exhibits greater pressure dependence than sandstone over this pressure range. Large low-frequency permittivities are due to grain-electrolyte interactions.

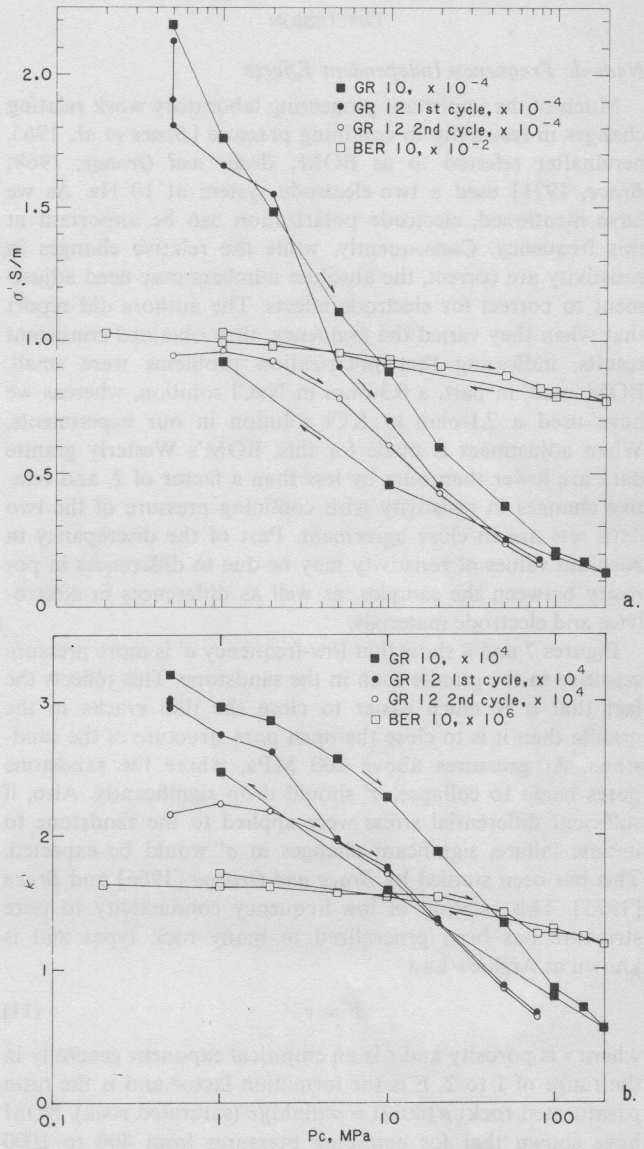

Fig. 8. Plot of (*a*) σ' and (*b*) K′ versus P_c at 1 Hz. Low-pressure values for GR12 second cycle indicate that the sample had not fully equilibrated at the time of measurements.

DISCUSSION

Near-dc Frequency Independent Effects

Much of the important pioneering laboratory work relating changes in resistivity to confining pressure [*Brace et al.*, 1965, hereinafter referred to as BOM; *Brace and Orange*, 1968; *Brace*, 1971] used a two-electrode system at 10 Hz. As we have mentioned, electrode polarization can be important at this frequency. Consequently, while the relative changes in resistivity are correct, the absolute numbers may need adjustment to correct for electrode effects. The authors did report that when they varied the frequency, they obtained consistent results, indicating that polarization problems were small. BOM used, in part, a 0.3-ohm m NaCl solution, whereas we have used a 7.1-ohm m KCl solution in our experiments. When adjustment is made for this, BOM's Westerly granite data are lower than ours by less than a factor of 2, and relative changes in resistivity with confining pressure of the two data sets are in close agreement. Part of the discrepancy in absolute values of resistivity may be due to differences in porosity between the samples, as well as differences in electrolytes and electrode materials.

Figures 7 and 8 show that low-frequency σ' is more pressure sensitive in the granite than in the sandstone. This reflects the fact that it is much easier to close the thin cracks in the granite than it is to close the open pore structure of the sandstone. At pressures above 200 MPa, where the sandstone pores begin to collapse, σ' should drop significantly. Also, if sufficient differential stress were applied to the sandstone to initiate failure, significant changes in σ' would be expected. This has been studied by *Brace and Orange* [1966] and *Brace* [1975]. This relation of low-frequency conductivity to pore structure has been generalized to many rock types and is known as Archie's Law

$$F = v^{-r} \tag{11}$$

where v is porosity and r is an empirical exponent generally in the range of 1 to 2. F is the formation factor and is the ratio ρ'(saturated rock)/ρ'(fluid) $\simeq \sigma'$(fluid)/σ'(saturated rock). BOM have shown that for confining pressures from 400 to 1000 MPa, $r = 2$ provides a very good fit to many rock types, although for lower confining pressure, where crack porosity was significant, values of r were lower. For example, at 5 MPa, their Westerly granite fit $r = 1.5$. Estimates of r from our 1-MPa data for Westerly, Berea, and porous ceramic are, 1.3, 1.6, and 1.7, respectively. In our experiments we did not measure changes in porosity with confining pressure. However, by assuming sample GR10 had a similar porosity reduction to Westerly granite reported by BOM, we get $r = 2.1$ at 200 MPa. Thus our data, as well as BOM's data, suggest a gradual increase in r with increasing confining pressure for crystalline rocks in the region 0 to 400 MPa, the pressure range in which crack porosity is significant. While (11) provides a good approximation to a wide range of rock types, it does not appear capable of fully describing the pressure dependent changes of conductivity related to closure of high aspect ratio cracks.

Brace et al. [1968] and *Brace* [1977] compared the changes in resistivity and permeability due to changes in confining pressure. They reported a consistent relation over many orders of magnitude and for many rock types. In their theoretical analysis they related fluid flow, porosity, and electrical resistivity by combining Darcy's law and Poiseuille's law and assuming that fluid flow paths are the same as electrical conductivity paths in the rock:

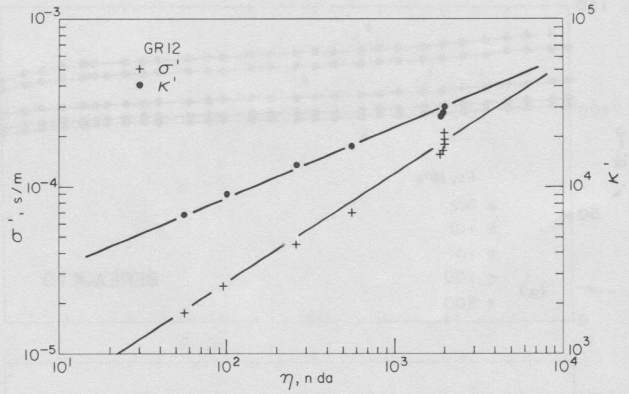

Fig. 9. Plot of σ' and K' versus permeability η for enhanced permeability sample GR12. Lines are least squares fits to data.

$$\eta = \frac{m^2}{k_0} F^{-2} v^{-1} \tag{12}$$

where k_0 is a shape factor which can vary between 2 and 3; m is hydraulic radius, which is the volume of the interconnected pores divided by their surface area. Brace et al. then expressed permeability in terms of porosity or formation factor by combining (11) and (12):

$$\eta = \frac{m^2}{k_0} v^{2r-1} = \frac{m^2}{k_0} F^{(1/r)-2} \tag{13}$$

For Westerly granite, m and k_0 were found to have little pressure dependence up to 200 MPa [*Brace*, 1977]. Because we measured permeability as a function of effective pressure for sample GR12, prior to performing the resistivity measurements, we can also compare η and σ'. The data are plotted in Figure 9. A least squares fit to the data gives a slope = 0.66 ± 0.02. For $r = 2$, (13) predicts a slope of 2/3. Thus as in the work of *Brace* [1977], (13) fits our data very well.

Relative permittivity K', at 1 Hz, is also plotted in Figure 9 and also obeys a power law. The mixing law (10) that applies to dry rocks [*Olhoeft and Strangway*, 1975; *Olhoeft*, 1980] is found to be inadequate to explain the very large measured low-frequency permittivities. These permittivities, which greatly exceed values for the bulk rock or electrolyte alone, are generally attributed to interfacial polarization phenomena at the grain-electrolyte boundaries and are not accounted for in this simple geometric mixing law. If we assume that permittivity (at fixed frequency) is proportional to wetted crack surface area, we can write

$$K' = cmvV_0 \frac{1}{m} \tag{14}$$

where V_0 is the volume of the sample and c is a proportionality constant. Combining (13) and (14), we get

$$\eta = \frac{1}{k_0} (cV_0)^{2r-1} m^{3-2r} K'^{(2r-1)} \tag{15}$$

As stated earlier, m is nearly constant for confining pressure up to 200 MPa. Assuming that $r = 2$, a plot of log K' versus log η should have a slope of 1/3. A least squares fit to the data in Figure 9 gives a slope of 0.41 ± 0.01 which agrees reasonably well with the predicted slope, given the simplicity of the model. If the above analysis proves to be applicable to rocks in general, then the measurement of low-frequency permittivity may be used to estimate crack surface area. This tech-

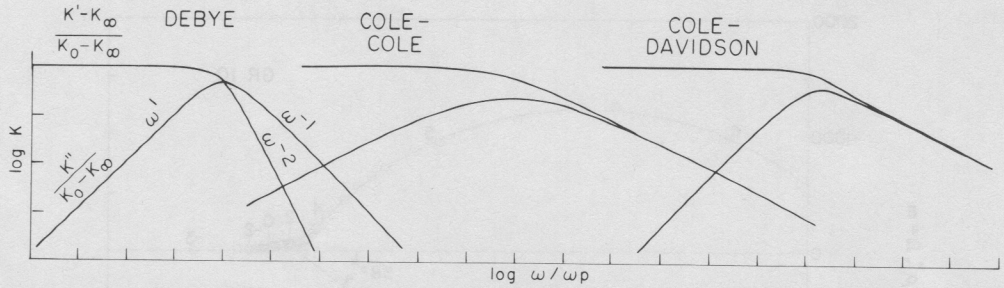

Fig. 10. Characteristic response functions $K^* - K_\infty$ in log-log presentation to stress the power law response for $\omega \neq \omega_p$. From left to right: Debye relaxation, Cole-Cole ($\alpha = 0.5$), and Cole-Davidson ($\beta = 0.5$). Plots are shifted horizontally for clarity.

nique could have applications in the laboratory as well as in the field, where, for example, it would be useful to monitor growth of microcracks in the dilatant source region of an impeding earthquake. These relations may prove useful for remote sensing applications, although more work needs to be done to determine how these parameters are interrelated in rock-electrolyte systems.

Frequency Dependent Models

Whereas σ' showed little frequency dependence below 1 kHz, K' displayed approximately a $1/\omega$ dependence in this range for both rock types. Large low-frequency permittivity has been reported primarily for clays, although it is observed in many saturated rocks [*Howell and Licastro*, 1961; *Arulanandan and Mitchell*, 1968; *Shahidi et al.*, 1975; *Lockhart*, 1980; *Keller*, 1982]. In fact, the occurrence of IP anomalies, commonly having decay times greater than 1 s, requires large low-frequency permittivities. Various models have been proposed to account for frequency dependent effects such as Warburg impedance which models interfacial grain-electrolyte interactions [*Wong*, 1979]. The following discussion will interpret our data in terms of a number of theoretical and empirical models including a relatively new model which is based on many-bodied interactions. Some of the more standard models have been extensively reviewed in the literature, but we present them here to discuss briefly some of the assumptions upon which they are based and the implications in applying them to our data.

Our present understanding of the microscopic dynamic response of dielectrics is based in large part on the work of Debye in the first half of this centruy. Debye analyzed the response of a charged dipole immersed in a viscous medium, arriving at

$$K^* = K_\infty + \frac{K_0 - K_\infty}{1 + i\omega\tau} \tag{16}$$

where

$$K_0 = \lim_{\omega \to 0} K'$$

$$K_\infty = \lim_{\omega \to \infty} K'$$

and τ is the relaxation time of the polarization process and is related to the viscosity of the medium. In terms of the time domain response, a step function change in **E** would result in an exponential decay in **J** with relaxation time τ. Equation (16) describes a complex frequency response function of characteristic shape shown in Figure 10, normalized by $K_0 - K_\infty$ and by $\omega_p = 1/\tau$. Parameter ω_p is the peak loss frequency corresponding to the maximum in K''. Classic Debye response has the characteristics that for $\omega \ll \omega_p$, K' approaches K_0 and $K'' \propto \omega$; and for $\omega \gg \omega_p$, $K' \propto \omega^{-2}$ and $K'' \propto \omega^{-1}$. It has long been recognized [*Cole and Cole*, 1941] that classical Debye response can only provide an approximation to the response of most solids and liquids, although these materials generally display a loss peak as well as dispersion of K'. *Cole and Cole* [1941] proposed an empirical expression, in an attempt to fit the observed response functions, of the form

$$K^* = K_\infty + \frac{K_0 - K_\infty}{1 + (i\omega\tau)^{1-\alpha}} \qquad 0 \leq \alpha \leq 1 \tag{17}$$

where α is the Cole-Cole distribution parameter. For $\alpha = 0$, this reduces to the Debye response but has the added feature that for increasing α, the distribution broadens and the peak loss decreases. The additional degree of freedom in the Cole-Cole distribution allows this model to fit the observed response functions better, although many other response functions have been proposed [i.e., *Davidson and Cole*, 1951] as either empirical fits or on the basis of specific models for dipole interactions. For a more complete comparison of various susceptibility functions, refer to *Hill and Jonscher* [1983]. Plots of Cole-Cole and Cole-Davidson response functions are shown in Figure 10 for $\alpha = \beta = 0.5$ where the Cole-Davidson response function is

$$K^* = K_\infty + \frac{K_0 - K_\infty}{(1 + i\omega\tau)^\beta} \qquad 0 \leq \beta \leq 1 \tag{18}$$

As can be seen in Figure 7*b*, no model of this type adequately describes our data. A plot of $K^*(\omega)$ in the complex plane has become a standard way of presenting permittivity data. Such a Cole-Cole plot of a single relaxation Debye response plots as a semicircle, centered on the real axis with diameter $K_0 - K_\infty$. The introduction of a distribution of relaxations (Cole-Cole distribution) has the effect of depressing the center of the circular arc below the real axis. When a response function such as the Cole-Davidson function, which produces asymmetric dispersion of K'' about the loss peak, is plotted, the result is no longer a circular arc, but rather an arc which is skewed toward higher K'. One characteristic of a Cole-Cole plot is that it emphasizes features near the loss peak at the expense of those occurring at very high and low frequencies. In fact, for some classes of response functions, Cole-Cole plots are of little value. This is the case for our data, which are in part dominated by large low-frequency disperison of permittivity (Figure 7*b*). None of the models discussed so far include this type of response. An alternative representation to the Cole-Cole plot is an Argand diagram (Figure 11) in which $\rho^*(\omega)$ is plotted in the complex plane. This proves more useful

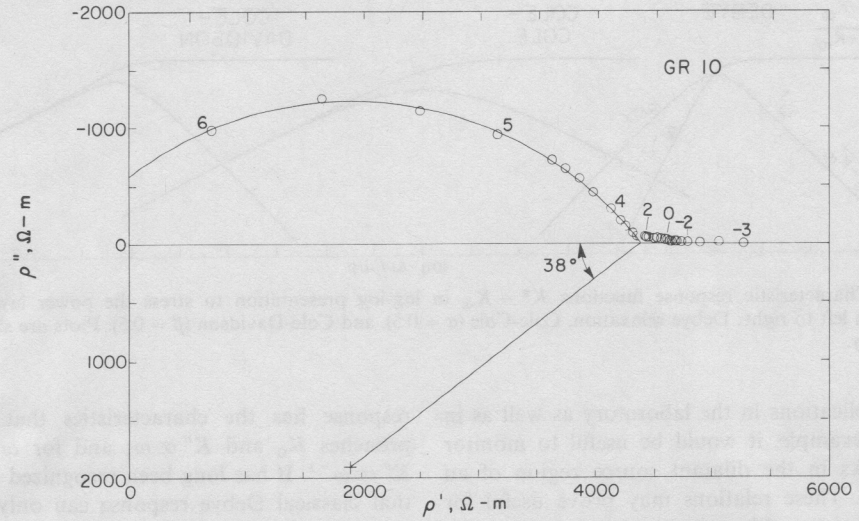

Fig. 11. Argand diagram for Westerly granite at $P_c = 0.5$ MPa. Log f is shown for selected frequencies. High-frequency data ($f > 1$ kHz) exhibit Cole-Cole type response, while low-frequency data display strong dispersion.

in displaying data such as ours, since low-frequency dispersion, when presented in this manner, does not dominate the plot. An Argand diagram has many of the properties of a Cole-Cole plot in that a Debye response generates a semicircle, whereas a Cole-Cole response will again depress the center of the circular arc below the real axis. In Figure 11, data for granite sample GR10 at 0.5 MPa is plotted. Log (f) is shown on the plot for selected frequencies. A circular arc fit to the high-frequency data gives a center depressed below the axis by 38° and $\omega_p = 2\pi f_p = 2.1 \times 10^6$ s^{-1}. The low-frequency data, however, diverge from the circular arc, again reflecting the strong dispersion and making a precise determination of dc conductivity impossible.

Low-frequency dispersion is often observed in high-temperature ionic conductors such as glasses as well as in rocks. In ionic conductors, the motions of hopping charges have been used to explain this effect [*Jonscher*, 1974], whereas in rock-electrolyte systems, the low-frequency dispersion is generally interpreted in terms of interfacial polarization, using models loosely collected under the general heading of Maxwell-Wagner effects [*Duhkin*, 1971]. The classical Maxwell-Wagner response was developed to model a system in which a small volume fraction of one material was dispersed in a medium of different permittivity and/or conductivity. In this case, charge carriers would migrate through the two materials until they encountered an interface, at which point they would tend to pile up. The resulting response function has the same form as the Debye single relaxation response. For common rock-water systems such as ours, the critical frequency ω_p, computed from this classical Maxwell-Wagner model, is of the order of 10^8 s^{-1}. By increasing the volume fraction of the dispersed material, allowing for mutual interaction of the dispersed inclusions, and altering the shape and size of the inclusions, more complicated response functions can be generated, although none of these added features properly models a saturated rock which includes tortuous, interconnected conducting paths. Another class of models was developed [*Overbeek*, 1952; *Schwarz*, 1962; *van Beek*, 1967; *Duhkin*, 1971; *Hasted*, 1973] which recognized the role of surface conduction and polarization of charge carriers trapped in the boundary layers of particles in colloidal suspensions. While this mechanism may account for the slight increase in phase angle for the Berea sample at 0.1 Hz (due to the small percentage of clay in this sample), it does not account for the major features observed in our experiments.

Many-Bodied Model

The strong low-frequency dispersion observed in both the granite and sandstone samples, characterized in Figures 4–6 by a nearly constant phase angle of −10 mrad, is one of the main features of the data. The difficulty in modeling this with a distributed relaxation-type model is that it requires postulation of a very broad, flat distribution of relaxation times covering orders of magnitude of frequency. An alternative approach to the description of dielectric response which has received little attention in the geophysical community has been presented by Hill, Jonscher, Dissado, and colleagues [*Hill and Jonscher*, 1983; *Jonscher*, 1981; *Dissado and Hill*, 1983]. Upon examining response functions of samples exhibiting a broad range of dielectric behavior, they have proposed a "universal" dielectric response model (hereinafter referred to as HJD) capable of describing the response of dielectrics from the millikelvin range to temperatures near phase transitions of the materials. This model is based on analysis of many-bodied interactions and preserves, as special cases, response functions such as the Debye, Cole-Cole, and Cole-Davidson. The HJD model allows for ions or structural elements to make sudden, low-energy transitions which will result in a much slower readjustment of the surrounding structure. In this way, while little energy is required for the initial transition, a much larger total energy can be distributed over the surrounding structure as it readjusts. This process is termed configurational tunneling. The HJD model is a two-parameter model predicting power law response on either side of the peak loss frequency ω_p. According to their model the response function has the properties that

$$K' - K_\infty \propto \omega^{-(1-n)} \qquad \omega > \omega_p \qquad (19a)$$

$$K'' \propto \omega^{-(1-n)} \qquad \omega > \omega_p \qquad (19b)$$

$$K_0 - K_\infty - a(K' - K_\infty) \propto \omega^m \qquad \omega < \omega_p \qquad (19c)$$

$$K'' \propto \omega^m \qquad \omega < \omega_p \qquad (19d)$$

where $0 \leq m, n \leq 1$. The HJD parameters can be interpreted

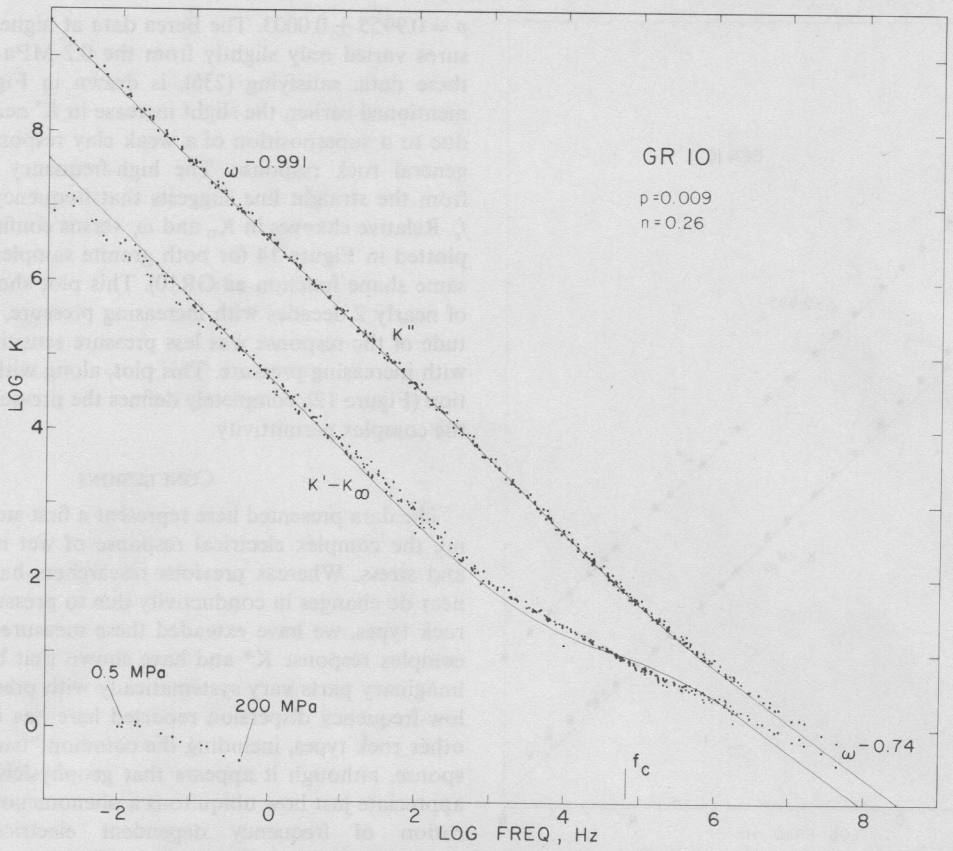

Fig. 12. Log-log plot of $K^* - K_\infty$ versus f for GR10 with all pressures superimposed to give composite plot. Datum plotted in lower left corner shows the required translation of successive data sets (see text). Theoretical fit from *Dissado and Hill* [1984] is also plotted.

in terms of local configurational processes that occur during relaxation [*Dissado and Hill*, 1983] and can reflect such properties as degree of local structure, amount of impurities, and fluid viscosity. It is important to distinguish between low-frequency dispersion in which K^* obeys (19*a*) and (19*b*) and the presence of dc conduction in which

$$K' = K_0 \qquad \omega < \omega_p \tag{20a}$$

$$K'' = \frac{\sigma_{dc}}{\varepsilon_0 \omega} \qquad \omega < \omega_p \tag{20b}$$

Since n in (19*b*) is often very small, it is difficult to distinguish between these two classes from the frequency response of $K''(\omega)$ alone. The low-frequency dispersion response is distinguished primarily by the power law dependence of $K' - K_\infty$.

Low-Frequency Dispersion Model

Jonscher [1978] and *Dissado and Hill* [1984] have recognized a special class of dielectric response which they refer to an anomalous low-frequency dispersion and which, in fact, provides a good description of our data. In this class of materials, the frequency dependence of (19*a*) persists throughout a transition from a small value of the index n to a different, and larger, value beyond a characteristic frequency ω_c. We will follow the convention of *Dissado and Hill* [1984] and define the value of $(1 - n)$ at the lower frequency as p. This dispersion phenomenon has been observed in a number of materials including high-temperature ionic conductors such as glasses [*Jonscher*, 1974] as well as in wet rocks and other geological materials [*Jonscher*, 1978]. The low-frequency dispersion model, developed to fit data of this form, assumes a process in which transport of charge is accomplished by site hopping of charge carriers in response to an applied field. The charge carriers are assumed to move in a system that has some degree of local order (local clusters) and contains partially filled ion-binding sites. The movement of charge carriers to new sites within a cluster (in which constraints are imposed owing to the degree of structural coherence) and movement to sites in new clusters (in which no structural coherence exists between donor and receiver sites) result in two relaxation processes. *Hill and Jonscher* [1983] have shown that relaxation behavior generally obeys the functional form

$$K^* = K_0 F(\omega/\omega_c) \tag{21}$$

in which $F(\ )$ is a complex spectral shape function normalized with respect to peak loss frequency or, in the case of low-frequency dispersion, critical frequency. *Dissado and Hill* [1984] developed an analytic expression for the low-frequency dispersion spectral shape function:

$$F(\omega/\omega_c) = \left(\frac{\omega_c}{\omega_c + i\omega}\right)^{1-n} {}_2F_1\left(1 - n,\, 1 + p;\, 2 - n;\, \frac{\omega_c}{\omega_c + i\omega}\right) \tag{22}$$

in which ${}_2F_1\ (;\ ;)$ is the Gaussian hypergeometric function. In order to compare this model with our data, we use the fact that if $K^*(\omega)$ is measured at two different temperatures or pressures, the response function will have the same form and will simply be scaled by the changes in K_0 and ω_c. This

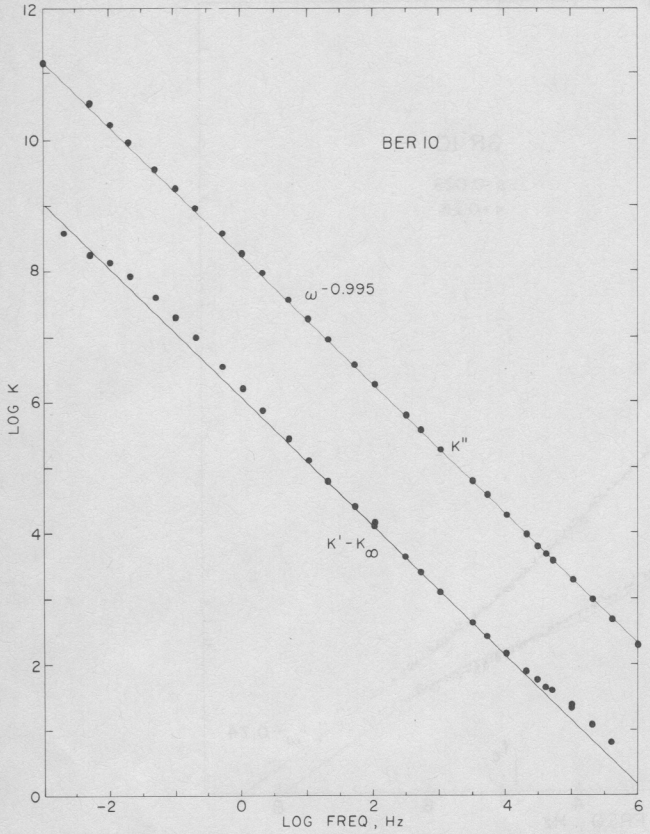

Fig. 13. Log-log plot of $K^* - K_\infty$ versus f for BER10 at 0.2 MPa. Theoretical curve is also drawn.

implies that by using a log-log presentation, successive experiments under altered conditions can be superimposed by a simple translation of the data. Such a plot is presented in Figure 12 for all data for sample GR10 and in Figure 13 for 0.2-MPa data for sample BER10. The values of K_∞ used in these plots are estimated by extrapolating the high-frequency permittivities to $K'' = 0$. The values of K_∞ for GR10, GR12, and BER10 are 9.7, 9.4, and 22.8, respectively. These are independent of confining pressure to within the 4% estimated accuracy. In Figure 12 the axes are labeled correctly for the GR10 data at 0.5 MPa. The symbols in the lower left corner of the plot show the shift in position of a single datum resulting from the translation of each data set (due to changing confining pressure). It can be seen that the granite data, taken at different confining pressures, all exhibit the same spectral shape function. The HJD parameters n and p can be estimated most accurately from the asymptotic relations

$$\frac{K' - K_\infty}{K''} = \tan\left[\frac{n\pi}{2}\right] \qquad \omega > \omega_c \qquad (23a)$$

$$\frac{K' - K_\infty}{K''} = \tan\left[\frac{(1-p)\pi}{2}\right] \qquad \omega < \omega_c \qquad (23b)$$

This results in $n = 0.26 \pm 0.06$ and $p = 0.991 \pm 0.003$ for the GR10 data. The theoretical fit (22) to the data is plotted in Figure 12 with $f_c = 2\pi\omega_c = 6.8 \times 10^4$ Hz. Dissado and Hill relate the parameters n and p to the local structure controlling the motion of charge carriers in the sample. The plot of the Berea permittivity (Figure 13) indicates that all data were taken below ω_c so that n cannot be determined but $p = 0.9955 \pm 0.0003$. The Berea data at higher confining pressures varied only slightly from the 0.2-MPa data. The fit to these data, satisfying (23*b*), is drawn in Figure 13. As was mentioned earlier, the slight increase in K' near 0.1 Hz may be due to a superposition of a weak clay response on top of the general rock response. The high-frequency deviation of K' from the straight line suggests that frequency is approaching f_c. Relative changes in K_0 and ω_c versus confining pressure are plotted in Figure 14 for both granite samples (GR12 had the same shape function as GR10). This plot shows a drop in ω_c of nearly 2 decades with increasing pressure, while the amplitude of the response was less pressure sensitive and increased with increasing pressure. This plot, along with the shape function (Figure 12), completely defines the pressure dependence of the complex permittivity.

Conclusions

The data presented here represent a first step in understanding the complex electrical response of wet rocks to pressure and stress. Whereas previous researchers have examined the near dc changes in conductivity due to pressure for numerous rock types, we have extended these measurements to the full complex response K^* and have shown that both the real and imaginary parts vary systematically with pressure. The strong low-frequency dispersion reported here has been observed in other rock types, including the common "background" IP response, although it appears that geophysicists have failed to appreciate just how ubiquitous a phenomenon it is. The application of frequency dependent electrical response to earthquake-related phenomena still requires much work, although the low-frequency effects are important in modeling such phenomena as earthquake lights [*Lockner et al.*, 1983; *Lockner and Byerlee*, 1985]. While many of the details of the electrical response of wet granite and sandstone systems have

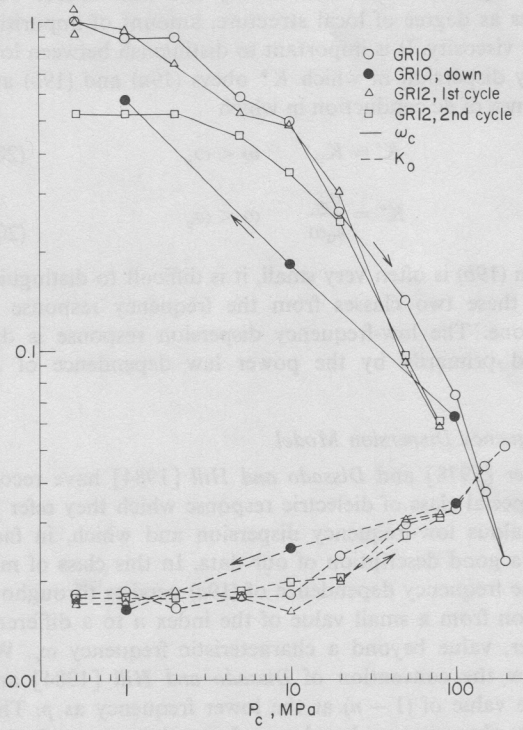

Fig. 14. Relative change of ω_c and K_0 versus P_c for both granite samples.

been worked out, more complicated systems such as clays and fault gouge still need to be examined in detail before earthquake-related electrical phenomena can be fully understood and exploited.

Acknowledgment. We thank Gary Olhoeft for all of his help and patience in developing the measurement system used in these experiments.

REFERENCES

Arulanandan, K., and J. Mitchell, Low frequency dielectric dispersion of clay-water-electrolyte systems, *Clays Clay Miner., 16*, 337–351, 1968.

Brace, W. F., Resistivity of saturated crustal rocks to 40 km based upon laboratory measurements, in *The Structure and Physical Properties of the Earth's Crust, Geophys. Monogr. Ser.*, vol. 14, edited by J. G. Heacock, pp. 243–255, AGU, Washington, D C., 1971.

Brace, W. F., Dilatancy related electrical resistivity changes in rocks, *Pure Appl. Geophys., 113*, 207–217, 1975.

Brace, W. F., Permeability from resistivity and pore shape, *J. Geophys. Res., 82*, 3343–3349, 1977.

Brace, W. F., and A. S. Orange, Electrical resistivity changes in saturated rock under stress, *Science, 153*, 1525–1526, 1966.

Brace, W. F., and A. S. Orange, Further studies of the effects of pressure on electrical resistivity of rocks, *J. Geophys. Res., 73*, 5407–5420, 1968.

Brace, W. F., A. S. Orange, and T. R. Madden, The effect of pressure on the electrical resistivity of water-saturated crystalline rocks, *J. Geophys. Res., 70*, 5669–5678, 1965.

Brace, W. F., J. B. Walsh, and W. T. Frangos, Permeability of granite under high pressure, *J. Geophys. Res., 73*, 2225–2236, 1968.

Cole, K. S., and R. H. Cole, Dispersion and adsorption in dielectrics, I, alternation current characteristics, *J. Chem. Phys., 9*, 341–351, 1941.

Davidson, D. W., and R. H. Cole, Dielectric relaxation in glycerol, propylene glycol, and *n*-propanol, *J. Chem. Phys., 29*, 1484–1490, 1951.

Dissado, L. A., and R. M. Hill, A cluster approach to the structure of imperfect materials and their relaxation spectroscopy, *Proc. R. Soc. London, Ser. A, 390*, 131–180, 1983.

Dissado, L. A., and R. M. Hill, Anomalous low-frequency dispersion, *J. Chem. Soc. Faraday Trans. 2, 80*, 291–319, 1984.

Duhkin, S. S., Dielectric properties of disperse systems, in *Surface and Colloid Science*, vol. 3, edited by E. Matijevic, pp. 83–166, John Wiley, New York, 1971.

Frisillo, A. L., G. R. Olhoeft, and D. W. Strangway, Effects of vertical stress, temperature and density on the dielectric properties of lunar samples 72441, 12, 15301, 38 and a terrestrial basalt, *Earth Planet. Sci. Lett., 24*, 345–356, 1975.

Hasted, J. B., *Aqueous Dielectrics*, Chapman and Hall, London, 1973.

Hermance, J. F., and J. Pedersen, Deep structure of the Rio Grande Rift: A magnetotelluric interpretation, *J. Geophys. Res., 85*, 3899–3912, 1980.

Hill, R. M., and A. K. Jonscher, The dielectric behavior of condensed matter and its many-body interpretation, *Contemp. Phys., 24*, 75–110, 1983.

Howell, B. F., and P. H. Licastro, Dielectric behavior of rocks and minerals, *Am. Mineral., 46*, 269–288, 1961.

Jonscher, A. K., Hopping losses in polarizable dielectric media, *Nature, 250*, 191–193, 1974.

Jonscher, A. K., Low-frequency dispersion in carrier-dominated dielectrics, *Philos. Mag. Part B, 38*, 587–601, 1978.

Jonscher, A. K., A new understanding of the dielectric relaxation of solids, *J. Mater. Sci., 16*, 2037–2060, 1981.

Keller, G. V., Electrical properties of rocks and minerals, in *Handbook of Physical Properties of Rocks*, vol 1, edited by R. S. Carmichael, 404 pp., CRC Press, Boca Raton, Fla., 1982.

Keller, G. V., and F. C. Frischknecht, *Electrical Methods in Geophysical Prospecting*, Pergamon, New York, 1966.

Lockhart, N. C., Electrical properties and the surface characteristics and structure of clays, I, Swelling clays, *J. Colloid Interface Sci., 74*, 520–529, 1980.

Lockner, D. A., and J. D. Byerlee, Complex resistivity of fault gouge and its significance for earthquake lights and induced polarization, *Geophys. Res. Lett., 12*, 211–214, 1985.

Lockner, D. A., M. J. S. Johnston, and J. D. Byerlee, A mechanism for the generation of earthquake lights, *Nature, 302*, 28–33, 1983.

Madden, T. R., High sensitivity monitoring of resistivity and self-potential variations in the Hollister and Palmdale areas for earthquake prediction studies, in *Summaries of Technical Reports*, vol. 17, pp. 355–358, *Open File Rep. 83-918*, National Earthquake Hazards Reduction Program, U.S. Geological Survey, Washington, D. C., 1983.

Madden, T. R., and R. Cantwell, Induced polarization, a review, *Min. Geophys., 2*, 373–400, 1967.

Morrison, H. F., The study of temporal resistivity variations on the San Andreas fault, in *Summaries of Technical Reports*, vol. 6, pp. 250–251, National Earthquake Hazards Reduction Program, U.S. Geological Survey, Washington, D. C., 1978.

Nelson, P., and G. Van Voorhis, Estimation of sulfide content from induced polarization data, *Geophysics, 48*, 62–75, 1983.

Olhoeft, G. R., Electrical properties, Initial Reports on the Petrophysics Laboratory, *U.S. Geol. Surv. Circ., 789*, 1–25, 1979*a*.

Olhoeft, G. R., Nonlinear electrical properties, in *Nonlinear Behavior of Molecules, Atoms and Ions in Electric, Magnetic or Electromagnetic Fields*, edited by L. Neel, pp. 395–410, Elsevier, New York, 1979*b*.

Olhoeft, G. R., Electrical properties of rocks, in *Physical Properties of Rocks and Minerals*, edited by Y. S. Touloukian, W. R. Judd, and R. F. Roy, McGraw-Hill, New York, 1980.

Olhoeft, G. R., Electrical properties of granite with implications for the lower crust, *J. Geophys. Res., 86*, 931–936, 1981.

Olhoeft, G. R., and D. W. Strangway, Electrical properties of the first 100 meters of the moon, *Earth Planet. Sci. Lett., 24*, 394–404, 1975.

Overbeek, J. T. G., The interaction between colloidal particles, in *Colloid Science I*, edited by H. Kruyt, p. 240, Elsevier, New York, 1952.

Parkhomenko, E. I., Electrical resistivity of minerals and rocks at high temperature and pressure, *Rev. Geophys. Space Phys., 20*, 193–218, 1982.

Rikitake, T., and Y. Yamazaki, A resistivity precursor of the 1974 Izu-Hanto-Oki earthquake, *J. Phys. Earth, 27*, 1–6, 1979.

Saint-Amant, M., and D. W. Strangway, Dielectric properties of dry, geological materials, *Geophysics, 35*, 624–645, 1970.

Schwan, H. P., Determination of biological impedances, in *Physical Techniques in Biological Research*, vol. 6, edited by W. Nastuk, pp. 323–407, Academic, New York, 1963.

Schwan, H. P., G. Schwarz, J. Maczuk, and H. Pauly, On the low-frequency dielectric dispersion of colloidal particles in electrolyte solutions, *J. Phys. Chem., 66*, 2626–2635, 1962.

Schwarz, G., A theory of the low-frequency dispersion of dielectric particles in electrolyte solution, *J. Phys. Chem., 66*, 2636–2642, 1962.

Scott, J., R. Carroll, and D. Cunningham, Dielectric constant and electrical conductivity measurements of moist rock: A new laboratory method, *J. Geophys. Res., 72*, 5101–5115, 1967.

Shahidi, M., J. B. Hasted, and A. K. Jonscher, Electrical properties of dry and humid sand, *Nature, 258*, 596–597, 1975.

Stanley, W. D., J. E. Boehl, F. X. Bostick, and H. W. Smith, Geothermal significance of magnetotelluric sounding in the eastern Snake River Plain–Yellowstone region, *J. Geophys. Res., 82*, 2501–2514, 1977.

Sumi, F., The induced polarization method in ore investigation, *Geophys. Prospect., 19*, 459–477, 1961.

Ucok, H., Temperature dependence of the electrical resistivity of aqueous salt solutions and solution-saturated rocks, Ph.D. thesis, 154 pp., Univ. of Southern Calif., Los Angeles, 1979.

Van Beek, Dielectric behavior of heterogeneous systems, in *Progress in Dielectrics*, vol. 7, edited by J. B. Birks, pp. 69–114, Heywood, London, 1967.

Von Hippel, A. R., *Dielectric Materials and Applications*, 438 pp., MIT Press, Cambridge, Mass., 1954.

Wong, J., An electrochemical model of the induced-polarization phenomenon in disseminated sulfide ores, *Geophysics, 44*, 1245–1265, 1979.

J. D. Byerlee and D. A. Lockner, U.S. Geological Survey, 345 Middlefield Road, MS 977, Menlo Park, CA 94025.

(Received September 6, 1984;
revised February 22, 1985;
accepted April 3, 1985.)